Adsorption 6, 33–45 (2000)

Adsorption Characteristics of Natural Erionite, Clinoptilolite and Mordenite Zeolites from Mexico

M.A. HERNÁNDEZ
Departamento de Química, Universidad Autónoma Metropolitana-Iztapalapa, P.O. Box 55-534, México 09340 D.F., México; Centro de Química (Ingeniería Química), Instituto de Ciencias, Universidad Autónoma de Puebla, Edif. 76, Complejo de Ciencias, Puebla 72570, México; Posgrado de Ciencias Ambientales, Instituto de Ciencias, Universidad Autónoma de Puebla, Puebla 72570, México

L. CORONA
Centro de Química (Ingeniería Química), Instituto de Ciencias, Universidad Autónoma de Puebla, Edif. 76, Complejo de Ciencias, Puebla 72570, México

F. ROJAS
Departamento de Química, Universidad Autónoma Metropolitana-Iztapalapa, P.O. Box 55-534, México 09340 D.F., México

Received March 11, 1998; Revised August 31, 1999; Accepted September 9, 1999

Abstract. Nitrogen sorption properties inherent to some natural zeolites from Mexico, such as erionites, clinoptilolites and mordenites, are determined and compared with corresponding sorption properties of homologous synthetic or acid modified forms. The mineralogies of natural zeolites are determined by X-ray analysis. N_2 low-pressure hysteresis loops are displayed by some substrata while are absent in others; key factors for this phenomenon to occur are the micropore structure and the ion-exchange treatment to which the natural precursors are subjected. Argon sorption at 76 K on selected samples evidence further the strong adsorption and the pore blocking effects at pore necks in the zeolites.

Keywords: natural zeolites, erionite, clinoptilolite, mordenite, low-pressure hysteresis

1. Introduction

For over 200 years, following their discovery by the Swedish chemist Cronstedt in 1756, zeolite minerals were considered to occur typically as minor constituents in vugs or cavities in basaltic and volcanic rocks. Nowadays there are more than forty known natural zeolites, but only some (e.g. ferrierite, phillipsite, chabazite, analcime, mordenite, erionite and clinoptilolite) have been used in catalytic applications (Michiels and De Herdt, 1987).

Zeolites are microporous materials with voids smaller than 2 nm (Sing et al., 1985). Micropores can be subdivided in *ultramicropores* (pore width lesser than 0.7 nm) and *supermicropores* (pore width between 0.7 and 2 nm) (Kaneko, 1997). The pore space of a zeolite is filled in a volumetric fashion (Dubinin and Astakhov, 1971) rather than a layer by layer mechanism, because of the close proximity of the surrounding pore walls to the adsorbate molecules. The sorption uptake increases with pressure; saturation of each pore domain with adsorbate molecules depends not only on

the size and shape of the microporous channels and cavities, but also on the size and geometry of the adsorptive molecule. For all these causes the structure of the adsorbed phase in micropores is then rather different than that developed in mesopores.

In the present work, N_2 sorption isotherms are analized by various methods in order to remark the particularities of the pore structure of some natural Mexican zeolites (erionites, clinoptilolites and mordenites). In general both primary (micro) and secondary (meso) porosities characterize these materials. The microporosity results from the specific crystalline structure of the zeolite which, in turn, depends upon composition. Unconverted matrix inserted between the zeolite particles causes the appearance of the secondary porosity, i.e., the presence of meso- and macropores (Tsitsihvili et al., 1992). The porosity can be measured by adsorption; the most usual and convenient adsorptive being nitrogen at 77 K.

The purpose of this work is to perform a series of comparative sorption studies between a natural zeolite and its homologous synthetic or modified form. This will allow the establishment of the extent of each kind of porosity in these zeolites. In addition some sorption particularities with regard to their microporous structures will be outlined. The set of zeolites chosen for this work involves 2-D (clinoptilolite, mordenite) and 3-D (erionite) porous networks consisting of channels of equal or different sizes interconnected to each other. N_2 and Ar sorption measurements will allow suggesting the causes for which low-pressure adsorption hysteresis is present in some of the zeolites while absent in others. The latter phenomenon will be ascribed to the structural and chemical properties of the substrata. Different methods of analysis of the sorption isotherms will be used to calculate the structural porous parameters and shed light about the possible filling stage mechanism undergone in each type of zeolite according to its pore structure.

1.1. Pore Structural Characteristics of Erionite, Clinoptilolite and Mordenite Zeolites

1.1.1. Erionite (Michiels and De Herdt, 1987). Erionite is a microporous material of wool-like appearance endowed of a three-dimensional intersecting channel system. All channels are equidimensional with elliptical 8-ring apertures and perpendicular to the *c*-axis. The zeolite is made of alternating cancrinite cages and hexagonal prisms arranged in connected columns. The

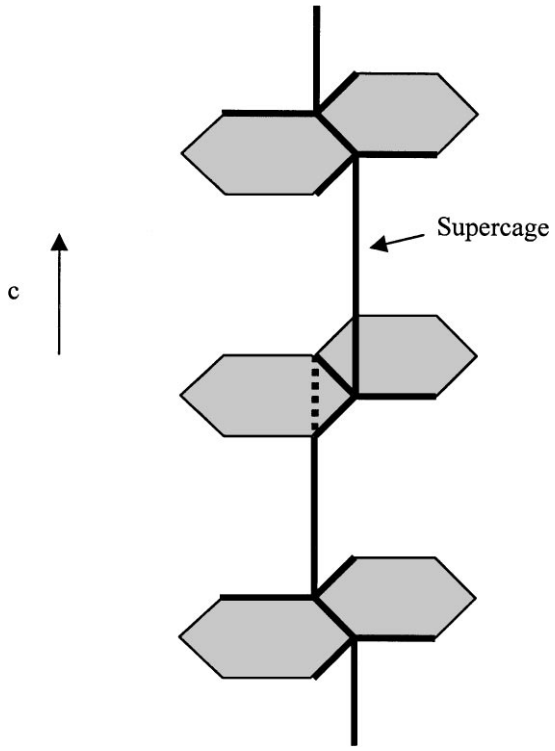

Figure 1. Schematic representation of the microporous structure of erionite.

cancrinite cages and hexagonal prisms enclose a pore cavity (supercage) with a length of 1.51 nm along the *c*-axis, molecules can enter this cavity through six 8-ring elliptical apertures. Cavities are interconnected via these six 8-ring elliptical openings of 0.36×0.51 nm to form the 3-D channel system. Molecules must diffuse in a zigzag path (see Fig. 1) since the main supercage channel in the *c*-direction does not run continuously (Breck, 1974).

The chemical composition of a type material is $(Na_2, Ca)_{3.5}K_2[Al_9Si_{27}O_{72}]\cdot 27H_2O$. The unit cell is hexagonal with parameters $a = b = 1.33$, $c = 1.51$ nm, $\alpha = 90^\circ$, $\beta = 90^\circ$, $\gamma = 120^\circ$. Substitution of sodium ions in the natural sample by calcium or hydrogen ions increases the sorption capacity of this zeolite.

1.1.2. Clinoptilolite (Tsitsihvili et al., 1992). Clinoptilolite is a member of the heulandite group of natural zeolites. The unit cell is monoclinic C-centered with Na^{1+}, K^{1+}, Ca^{2+} and Mg^{2+} as the most common charge-balancing cations. Unit cell parameters for the $(Na_{1.84}K_{1.76}Mg_{0.2}Ca_{1.24})(Si_{29.84}Al_{6.16}O_{72})\ 21.36H_2O$ form are $a = 17.662$ Å, $b = 17.911$ Å, $c = 7.407$ Å,

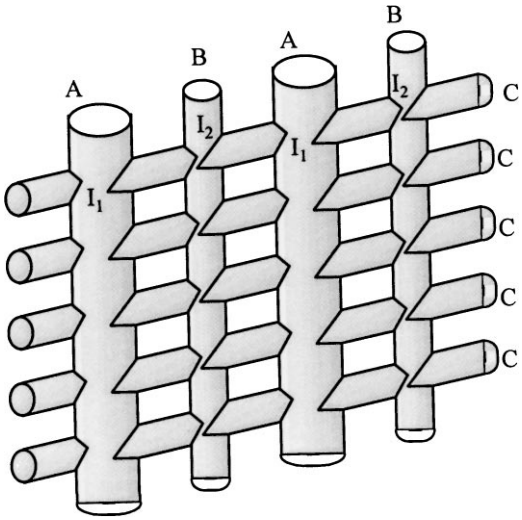

Figure 2. Clinoptilolite structure showing channels A, B and C and intersections I_1 and I_2.

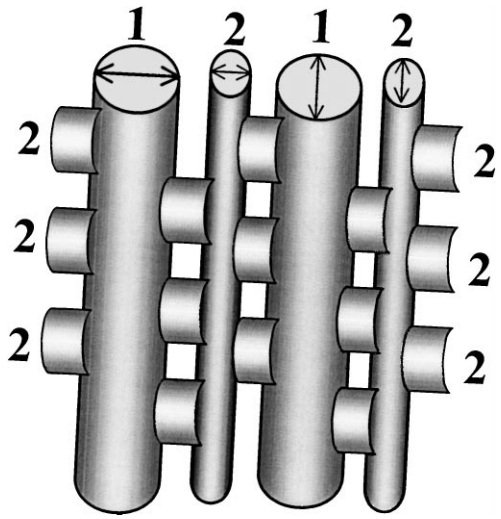

Figure 3. Schematic representation of the pore structure of mordenite. Numbers 1 and 2 represent the two types of channels in the zeolite.

and $\alpha = 90^\circ$, $\beta = 116.40^\circ$, $\gamma = 90^\circ$. Gas or vapour molecules penetrate the crystalline structure through a series of intersecting channels, each layer of channels separated by a dense, gas-impermeable layer of tetrahedra. Channels A (10-member rings, free diameters 0.44×0.72 nm) and B (8-member rings, free diameters 0.41×0.47 nm) are parallel to each other and to the *c*-axis of the unit cell, while C channels (8-member rings, free diameters 0.40×0.55 nm) run along the *a*-axis intersecting both A and B channels. Figure 2 illustrates the 2-D structure of clinoptilolite. The elliptic-shaped 8- and 10-member rings that form the channel system are non-planar. The existence of larger pores (i.e. supermicropores and mesopores) in natural and modified zeolites may be due to the existence of impurities or by partial removal of constituents of the zeolitic matrix during acid leaching. The type, number, and location of the charge-balancing cations residing in the A, B, and C channels influence the selectivity and uptake rate of gases by clinoptilolite.

1.1.3. Mordenite (Jacobs and Martens, 1987). Typical chemical composition of mordenite species is $Na_8[Al_8Si_{40}O_{96}]\cdot 24H_2O$; the unit cell is orthorhombic. Parameters of the simple mordenite cell vary between $a = 1.8052$–1.8168 nm, $b = 2.0527$ nm, $c = 0.7501$–0.7537 nm, $\alpha = \beta = \gamma = 90^\circ$. The Si/Al ratio is found between 4.5 and 5.5. Mordenite presents two types of porous channels. Channel 1 formed by the assemblage of 12-membered rings, each of which having 12 oxygen atoms. Channel 2 is in turn made of 8-membered rings in which there are 8 oxygen atoms. The porous structure of mordenite consists of a channel system in which 8- and 12-membered ring channels run parallel to the [001] or *c* axis and 8-membered ones parallel to [010] or *b* axis. Free diameters of the 12 membered rings are 0.65×0.70 nm, while free diameters of the 8-membered rings are 0.26×0.57 nm. Channels 1 and 2 are interconnected via perpendicular channel 2 tubes, in the form of small side pockets along the [010] axis. Thus the channel system is essentially a 2-dimensional network with elliptical 12-ring apertures and a *limiting diffusion* in the [010] or *b* direction. The mordenite channel structure can be visualised in Fig. 3. Cation sites reside in the centres of the 8-membered rings that are parallel either to *c* or *b*, these sites are regularly occupied thus leading to pore blocking and leaving the 12-membered channels as the only ones for molecular diffusion. It has been observed that mordenite allows the passage of molecules not greater than 0.42 nm. Natural mordenites, enriched with alkali cations, can be unblocked after treatment with dilute hydrochloric acid.

1.2. Adsorption on Microporous Solids

Adsorption on microporous solids shows at least two distinctive zones during the micropore filling (Gregg and Sing, 1982). In the first region (*primary process of*

micropore filling) there exists a considerable enhancement of the interaction potential between adsorbent and adsorbate molecules, so that pores (ultramicropores) become full at very low relative pressures (i.e. $p/p^0 \leq 0.01$). The interaction potential depends on the natures of the adsorptive and the adsorbent molecules. In the second region (*secondary process of micropore filling*, $0.01 \leq p/p^0 \leq 0.1$, 0.2) adsorption is not as sharp as in the first one, the enhancement of the interaction potential is not too high and the uptake of adsorptive molecules is mainly due to cooperative effects among them (i.e. there are attractive forces between adsorbate molecules that promotes adsorption). Adsorption in the first region is due to the ultramicropores whilst in the second region is related to the supermicropores. The second region gives rise to the rounded knee of the isotherm. These adsorption characteristics lead to a Type I isotherm. If in addition to micropores the adsorbent presents mesopores, the adsorption isotherm will now correspond to a Type IV with its characteristic high-pressure hysteresis loop.

Low-pressure hysteresis is also likely to be observed in microporous adsorbents and may be due to different causes such as (Mather, 1997):

(i) slow diffusion of the adsorbate molecules through the microporous constrictions, this would mean that adsorption equilibrium is not really reached during the time scale of the experiment and thus an apparent hysteresis is observed;
(ii) an inelastic distortion of the structure of the adsorbent, by swelling of its constituent particles or by the irreversible intercalation of adsorbate molecules within pores of molecular dimensions, as the adsorptive pressure is increased;
(iii) a strong irreversible bonding of the adsorbate to the adsorbent surface, especially at micropore constrictions. This also slows down the rate of molecular diffusion into the larger microporous cavities.

Strong irreversible adsorption of molecules is possible to occur at the canthi (corners at which pore walls meet) of microporous entities (Inagaki and Sunahara, 1997; Maddox et al., 1997). In the case of zeolites some corners would reside at the intersections of the porous channels, where strong adsorbate-adsorbent interactions have been predicted (Chiang et al., 1997). Furthermore, strong adsorption at these pore mouths will slow down the rate of diffusion into the micropore cavities and determine the appearance of the Dubinin-Astakhov (DA) or Dubinin-Radushkevich (DR) plots, since as it has already been pointed out (Stoeckli et al., 1998), the reduced accessibility of adsorptive molecules will reflect some of the particularities of the micropore size distribution or the presence of a *gate effect* at the entrance of the micropores.

1.3. Evaluation of Micropore and Mesopore Structural Parameters of Zeolites through Different Methods of Analysis

In this work substrata are erionites, clinoptilolites and mordenites; adsorptives are nitrogen and argon. The microporous volume, W_0, can be obtained from t, α_s or DR plots. The first two plots require of a reference isotherm on a non-porous substratum of similar chemical nature than the sample under analysis. Comparison between the standard and problem isotherms allows the evaluation of the total micropore adsorption and of the so-called *external area* (A_{ext}) of the adsorbent that is due to meso- and macropores. Convenient t or α_s standard isotherms have been provided for nitrogen or argon (Gregg and Sing, 1982). To calculate the thickness, $t/\text{Å}$ of the adsorbed layer of nitrogen as function of the relative vapour pressure p/p^0 the following Harkins-Jura (HJ) equation can be used:

$$t = \frac{13.99}{[0.034 + \log(p^0/p)]^{0.5}} \qquad (1)$$

Adsorption studies on microporous solids such as zeolites have shown that often the Dubinin-Radushkevich (DR) equation, applies in such systems:

$$W = W_0 \exp[-(RT \ln(p^0/p)/E_0]^2 \qquad (2)$$

W is the microporous volume filled at the relative pressure p/p^0 and W_0 is the total volume of the microporous space. $RT \ln(p^0/p)$ is the negative of the isothermal molar Gibbs free energy of transfer from the liquid at temperature T and saturation pressure p^0, to the adsorbate phase at equilibrium pressure p. E_0 is the characteristic energy of the solid and reflects the influence of the substratum on the amount adsorbed.

A DR plot is constructed by plotting $\ln(W)$ versus $\ln^2(p^0/p)$. In the case of truly microporous materials, a DR plot often exhibits a linear region extending over a wide range of relative pressures (e.g. 10^{-5}–0.2) and W_0 can be calculated from the intercept. A DR plot

requires adsorption data to be *corrected* for meso- and macropore adsorption, which would have contributed to the uptake at lower relative pressures (Gregg and Sing, 1982). This correction could be made if A_{ext} and the thickness of the adsorbed layer as function of the relative pressure, p/p^0, on a flat surface are known.

To provide micropore volumes in $cm^3\,g^{-1}$ it is common to assume the density of the adsorbate in the micropores as that of the saturated liquid. For nitrogen and argon at 76 K molar volumes of 34.41 $cm^3\,mol^{-1}$ and of 27.14 $cm^3\,mol^{-1}$ respectively can be taken as convenient values (WADD, 1961). The argon value corresponds to the density of the supercooled liquid.

For the type of natural zeolites studied here, the sorption data necessary to construct either a t- or α_s-plot usually lie between $0.1 < p/p^0 < 0.6$), a region significantly different from the location of data required to implement a DR plot (i.e. $p/p^0 < 0.2$). A good agreement between the DR and t micropore volume values would render a consistent analysis of the micro- and meso-porosities of the substratum.

A_{ext} can be also calculated from a method conceived by Remy and Poncelet (1995). In this method the microporous volume is subtracted from the adsorption values at relative pressures where all micropores have been already filled with adsorbate (i.e. $p/p^0 > 0.05$). This would allow obtaining a BET area corresponding to the external surface that, in principle, should render a good agreement with the values calculated from the t or α_s methods. If this subtraction is performed the linearity of the BET plot and the range of relative pressures at which the BET equation applies are be significantly extended. In addition to this the BET constant C_{BET} can change sign from negative (original data) to positive after subtraction of the micropore adsorption from the uptake data.

2. Experimental

2.1. Zeolite Samples

The zeolites used in this work are Mexican natural zeolites proceeding from different locations (see location and mineralogy in Table 1). There is one natural (CLIN) and one modified (CLIM) clinoptilolite samples, one natural (MORN) and one synthetic (MORS) mordenite specimens and one natural (ERIN) and one synthetic (ERIS) erionite substrata. MORS was purchased from Union Carbide and ERIS was prepared in the laboratory.[1]

Table 1. Source and mineralogy of natural zeolites.

Natural zeolite sample	Localization: town, state	X-ray characterization
ERIN	ERI TYPE Agua Prieta, Sonora	ERI-CLI
CLIN	CLI TYPE Tehuacán, Puebla	CLI-quartz
MORN	MOR TYPE Magdalena, Oaxaca	MOR-CLI

ERI ≡ erionite; CLI ≡ clinoptilolite; MOR ≡ mordenite.

Natural clinoptilolite CLIN was subjected to a modification ion-exchange procedure consisting in 12 washing cycles in order to obtain CLIM. Each washing cycle was made inside a burette provided with sintered glass filters and glass stopcocks; the zeolite was introduced and brought in contact with diluted 0.1 N HCl for two hours. This was followed by a rinse with deionized water to eliminate excess acid solution. The modifying procedure caused the interchange of polyvalent cations by protons, the dealumination of the structure and the removal of impurities.

2.1.1. Chemical Composition of the Zeolites. In order to evaluate the ratio Si/Al and especially to know the effect of acid treatment on dealumination of natural clinoptilolite (samples CLIN and CLIM) zeolites have been analysed by atomic absorption using a Perkin-Elmer Model 5000 instrument. Results are presented in Table 2.

2.1.2. X-Ray Diffraction Analysis. Samples were characterised by X-ray diffraction analysis using a Siemens D 500 apparatus. The zeolite specimens were classified according to recognised zeolitic types from the diffractograms obtained. Identification results are shown in Table 1. As example the diffraction patterns corresponding to natural (MORN) and synthetic (MORS) mordenites can be seen in Fig. 4. In general all the zeolites, including the natural substrata, exhibited good crystallinity and reasonable sharp diffraction patterns, especially the synthetic and modified forms.

2.1.3. Sorption Measurements. Nitrogen sorption isotherms were measured at 76 K in a vacuum/adsorption static volumetric apparatus (Quantachrome LC-1). A Micromeritics ASAP 2000 instrument was used to measure adsorption on MORS. A mesh-size distribution, i.e. 60–80 mesh, was chosen for every natural or synthetic specimen used for the adsorption

Table 2. Chemical compositions of erionite (ERI), clinoptilolite (CLI) and mordenite (MOR) zeolites.

Zeolite	SiO_2	Al_2O_3	Fe_2O_3	CaO	MgO	Na_2O	K_2O	Si/Al	Other
					ERI				
ERIN	59.45	11.17	2.40	0.60	0.85	4.55	3.80	4.69	17.18
ERIS	63.29	15.66	–	–	–	1.33	2.02	3.56	17.69
					CLI				
CLIN	67.07	11.31	1.21	3.57	0.68	2.90	0.52	5.22	12.74
CLIM	69.50	10.75	–	–	–	–	–	5.71	14.04
					MOR				
MORN	72.12	11.96	0.83	1.95	–	5.98	1.25	5.32	5.91

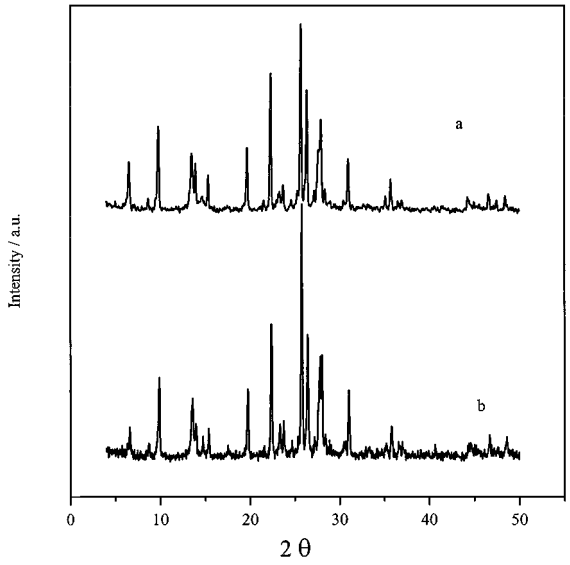

Figure 4. X-ray diffraction patterns of mordenites. (a) Natural MORN and (b) synthetic MORS samples.

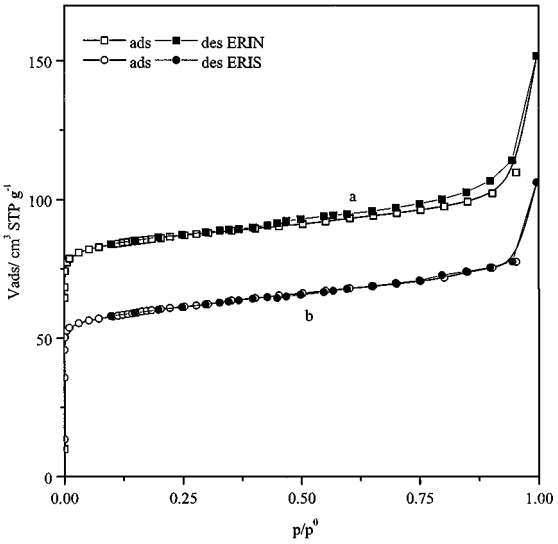

Figure 5. N_2 sorption at 76 K on erionites. (a) Natural ERIN and (b) synthetic ERIS.

measurements. Prior to the adsorption run, zeolites were vacuum treated at 300–350°C during 14 hours at a pressure smaller than 10^{-6} Torr.

Argon sorption isotherms at 76 K were determined in the same volumetric apparatus with the objective of having a more precise idea about the blocking effects existing at the constrictions of some of the adsorbents. Sample preparation was made in the same way as for nitrogen sorption.

3. Results and Discussion

3.1. Sorption Isotherms

Nitrogen sorption isotherms of the various zeolites studied in this work are shown in Figs. 5–7. In these figures the sorption isotherms of natural samples ERIN, CLIN and MORN can be visually compared with those of their homologous synthetic or modified samples ERIS, CLIM and MORS. All N_2 isotherms are either Type I or IV according to the IUPAC classification (Sing et al., 1985). Argon sorption isotherms measured on the natural and modified zeolites and labelled as ERINAr, CLIMAr and MORNAr are shown in Figs. 8–10. Ar isotherms are predominantly Type IV with a significant Type I contribution.

Textural results obtained from different analyses of these curves (BET, α_s, or t methods) are summarised in Table 3. In this table it has also been included the p/p^0 range that incorporates the data used to construct the BET and t plots and their corresponding linear correlation coefficients. Micropore volumes, W_0 ($cm^3\ g^{-1}$),

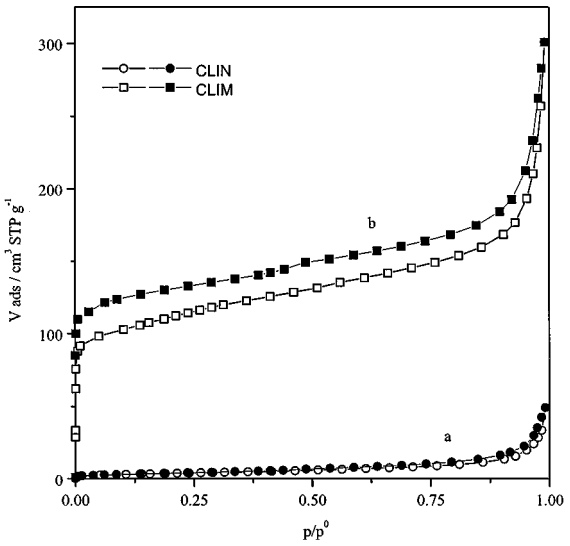

Figure 6. N_2 sorption at 76 K on clinoptilolites. (a) Natural CLIN and (b) modified CLIM.

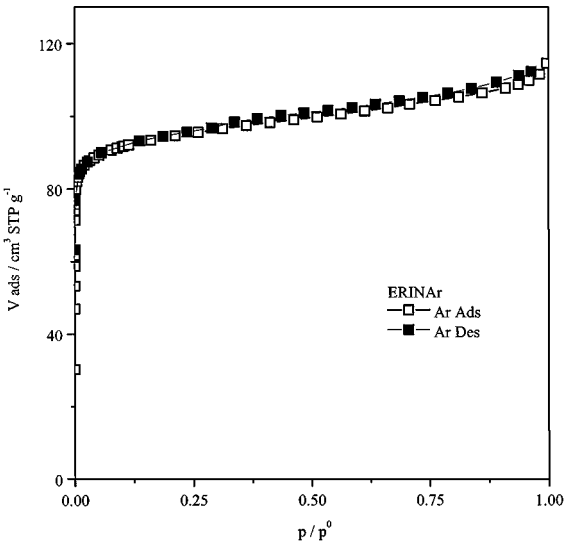

Figure 8. Ar sorption at 76 K on natural erionite ERIN.

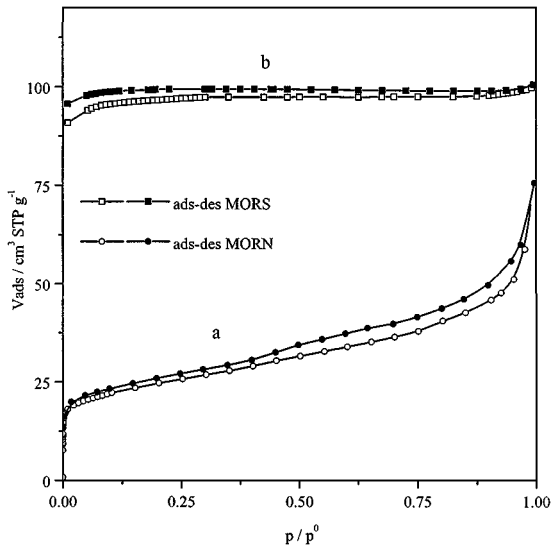

Figure 7. N_2 sorption at 76 K on mordenites. (a) Natural MORN and (b) synthetic MORS.

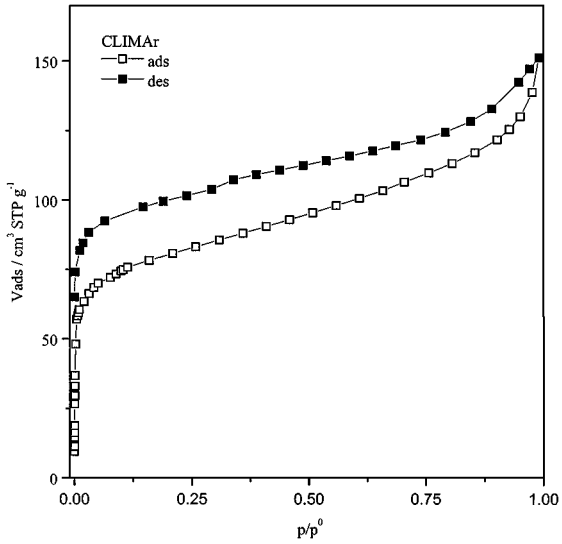

Figure 9. Ar sorption at 76 K on modified clinoptilolite CLIM.

have been calculated from the DR Eq. (2) and the t or α_s plots and are presented in Table 4. Specific sorption characteristics of the zeolitic types studied here are described below.

3.2. Erionites

N_2 and Ar sorption isotherms on both natural and synthetic erionite samples are shown in Figs. 5 and 8. An important point is that low-pressure hysteresis is not observed in neither sample. The synthetic sample originates a Type I isotherm, this isotherm being a reversible one. The shape of the isotherm of the natural sample is made of a combination of a Type I (micropores) and of a Type IV.

3.2.1. Nitrogen Sorption on Natural Erionite. This natural zeolite specimen displays a steep adsorption at low relative pressures ($p/p^0 \leq 10^{-4}$), showing afterwards a gradual (sloping) adsorption zone within the

Table 3. Some sorption parameters of natural, synthetic and modified zeolites.

Sample	A_B ($m^2\ g^{-1}$)	C_B	R (p/p^0 range)	$A_{B\,ext}$ ($m^2\ g^{-1}$)	$C_{B\,ext}$	R_{ext} (p/p^0 range)	A_t ($m^2\ g^{-1}$) (p/p^0 range)
ERIN	303.4	−138.1	0.9997 (0.05–0.15)	45.17	8.31	0.9999 (0.03–0.20)	48.39 (0.10–0.28)
ERINAr	283.7	−97.01	0.9997 (0.07–0.16)	38.80	14.67	0.9999 (0.10–0.25)	31.49 (0.31–0.66)
ERIS	197.5	−81.85	0.9998 (0.1–0.18)	57.83	102.1	0.9997 (0.03–0.22)	52.48 (0.03–0.35)
CLIN	13.60	65.21	0.9997 (0.05–0.36)	13.60	65.21	0.9997 (0.05–0.36)	15.47 (0.01–0.86)
CLIM	381.4	−201.3	0.9997 (0.05–0.21)	134.7	15.68	0.9997 (0.05–0.31)	119.5 (0.31–0.61)
CLIMAr	230.2	−83.26	0.9994 (0.08–0.26)	94.08	1.02	0.9998 (0.02–0.30)	95.45 (0.07–0.55)
MORN	120.5	8652	0.9999 (0.05–0.20)	55.19	125.2	0.9998 (0.01–0.30)	54.09 (0.02–0.40)
MORNAr	79.26	−130.4	0.9991 (0.05–0.26)	35.17	3.893	0.9997 (0.03–0.21)	31.13 (0.05–0.66)
MORS	331.7	−78.61	0.9996 (0.08–0.16)	12.95	56.10	0.9991 (0.13–0.28)	12.31 (0.17–0.29)

A_B, BET surface area; C_B, BET constant; R, BET linear correlation coefficient; $A_{B\,ext}$, BET external surface area; $C_{B\,ext}$, BET constant for adsorption on $A_{B\,ext}$; R_{ext}, BET linear correlation coefficient for adsorption on $A_{B\,ext}$; A_t, t-plot surface area. Argon surfaces areas have been calculated assuming 14.2 $Å^2$ as the average area occupied per molecule.

Table 4. Micropore-filling capacities of natural, synthetic and modified zeolites.

Sample	W_{0t}/$cm^3\ g^{-1}$ t-plot	W_{0DRC}/$cm^3\ g^{-1}$ DR corrected	W_{0DR}/$cm^3\ g^{-1}$ DR original
ERIN	0.1117	0.1122	0.1270
ERINAr	0.1310	0.1365	0.1399
ERIS	0.0694	0.0699	0.0867
CLIN	0.0000	0.0000	0.0048
CLIM	0.1236	0.1575	0.1614
CLIMAr	0.0631	0.0673	0.0851
MORN	0.0139	0.0156	0.0318
MORNAr	0.0274	0.0307	0.0339
MORS	0.1433	0.1439	0.1500

W_{0t}, microporous volume calculated from a t-plot; W_{0DRC}, microporous volume calculated from a DR plot using data corrected by adsorption on the external surface; W_{0DR}, DR microporous volume using the original adsorption data.

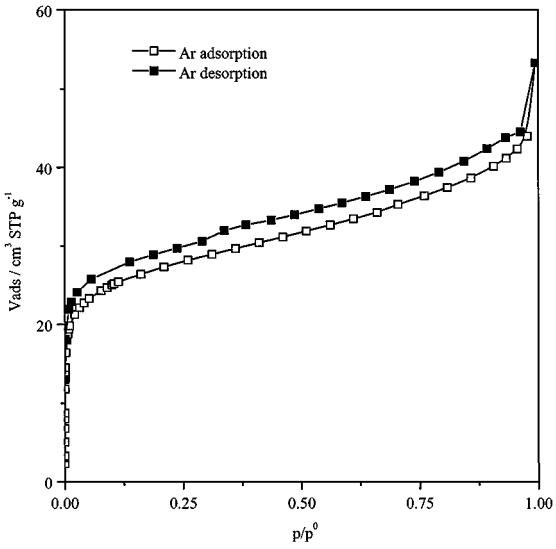

Figure 10. Ar sorption at 76 K on natural mordenite MORN.

range $10^{-4} < p/p^0 < 0.80$. This zone reflects both the total filling of the micropores (already accomplished at very low pressures) and the ongoing development of the adsorbed layer on the mesopores of the adsorbent. At even higher pressures there exists a second notable increase in the adsorption uptake, this time due to the occurrence of capillary condensation inside the mesopores of the sample. This latter part of the isotherm resembles adsorption on parallel plates (type H3 hysteresis loop in the IUPAC classification (Sing et al., 1985)) and may be likely due to the existence of lamellar impurities such as unconverted clay in between the zeolite crystallites.

Since low-pressure hysteresis is absent in this natural microporous solid N_2 molecules enter and exit reversibly, pore throats (i.e. the 8-ring elliptical windows that communicate the supercages in a zigzag pattern along the c-axis of the crystals) are large enough (0.36×0.51 nm) for the adsorptive N_2 molecules not to be irreversibly bounded at these channels intersections.

The DR plot (see Fig. 11) suggests that ultramicropore (channels) filling occurs at very low relative pressures (i.e. between 10^{-6} and 5×10^{-5}) since there is a prominent diminution of the uptake slope of the isotherm at around $p/p^0 = 5 \times 10^{-5}$. Supermicropores fill between $p/p^0 = 5 \times 10^{-5}$ and 10^{-2} (region at

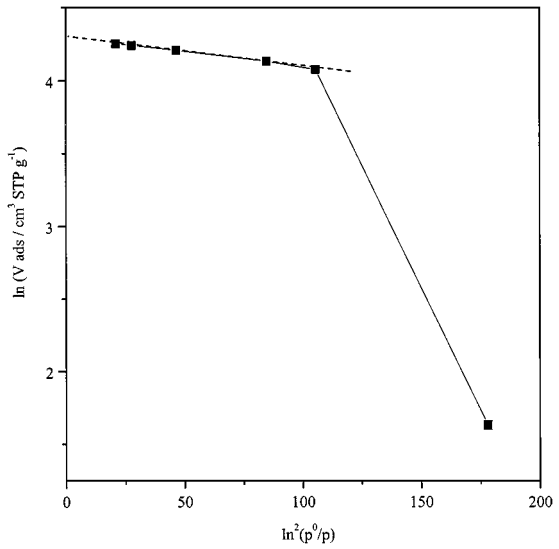

Figure 11. DR plot for N_2 adsorption on ERIN corrected for adsorption on the external surface.

which the DR plot is linear) and exist in a significantly smaller proportion than ultramicropores. Adsorption due to mesopores is evident from the t-plot where linearity can be observed between $p/p^0 = 0.10$ and 0.30. The microporous volumes calculated from the DR and t-plots are 0.1122 and 0.1117 $cm^3\,g^{-1}$ respectively. The DR plot has been constructed using a volume adsorbed corrected by adsorption on mesopores. The uncorrected DR plot renders a microporous volume of 0.1270 $cm^3\,g^{-1}$.

The BET surface area of the natural material is 303.4 $m^2\,g^{-1}$ (its linearity extends from $p/p^0 = 0.05$ to 0.15 with a correlation coefficient of 0.9997) and the external BET area (pressure range $p/p^0 = 0.03$ to 0.20, correlation coefficient 0.9999) is 45.17 $m^2\,g^{-1}$. For comparison the t-surface area is 48.39 $m^2\,g^{-1}$. Note that the linear region in the corrected BET plot now extends up to $p/p^0 = 0.20$ instead of 0.15 with the original data.

3.2.2. Argon Sorption on Natural Erionite. Ar sorption isotherm on sample ERIN at 76 K is shown in Fig. 8. There it can be observed the main features of the nitrogen isotherm are once more reproduced. There is no low-pressure hysteresis but instead an extremely narrow high-pressure hysteresis loop is displayed. So that there is also no irreversible adsorption of Ar in the channel system and lamellar impurities occur in a small amount. The BET area is 283.7 $m^2\,g^{-1}$ close to the nitrogen value of 303.4 $m^2\,g^{-1}$. The DR plot for Ar is rather different than for N_2 indicating lower interaction energy between the Ar molecules and the zeolite when compared to N_2. There is a linear region in this plot extending from $p/p^0 = 5 \times 10^{-4}$ up to 4×10^{-2}. W_0 the microporous volume is 0.1365 $cm^3\,g^{-1}$ and E_0 the adsorption energy is smaller than for nitrogen. The microporous volume calculated from the α_s plot is $W_0 = 0.1310$ $cm^3\,g^{-1}$, in good agreement with that obtained from the DR plot. The external surface area obtained from the t-plot is 31.49 $m^2\,g^{-1}$. The external BET area is 38.80 $m^2\,g^{-1}$ and the linear correlation coefficient is 0.9999.

3.2.3. Nitrogen Sorption on Synthetic Erionite. The synthetic erionite sample exhibits a smaller uptake capacity than the natural substratum. Low- and high-pressure hysteresis loops are practically absent in this zeolite. These features confirm the good purity and degree of crystallinity of the material. The N_2 sorption isotherm of the synthetic sample at 76 K is thus reversible throughout the whole range of relative pressures.

The filling of the 3-D channel system of synthetic erionite takes place mainly in the range of relative pressures between 10^{-6} and 10^{-4}, where more than 40% of the microporous space has become filled with adsorbate. The ultramicropores (i.e. the channel system of the erionite) start filling at very low relative pressures ($<10^{-6}$) up to about a relative pressure of 10^{-4} (this assertion is based upon the appearance of the isotherm at very low pressures). Supermicropores, which exist in a lesser extent than ultramicropores, fill between relative pressures of 10^{-4} and 10^{-2}.

Mesopores contribute slightly to the adsorption capacity of the sample and its extent can be evaluated from the t-plot. This t-plot is linear in the relative pressure range between 0.03 and 0.35. Thus supermicropores become filled before $p/p^0 = 0.05$, causing that the knee of the isotherm extends between $p/p^0 = 10^{-4}$ and 10^{-2} approximately. The DR plot is linear along the relative pressure range between 10^{-4} to 10^{-2}. If this plot is constructed by taking into account adsorption on the mesopores then a better agreement can be reached between the microporous volume rendered by this plot and the value obtained through the t-plot. Corresponding values are respectively 0.0699 and 0.0694 cm^3 per gram of zeolite (see Table 4) which are indeed very close to each other.

In summary the N_2 adsorption mechanism that occur in erionites may be described as follows. First the

adsorptive molecules start adsorbing at very low relative pressures in the ultramicroporous channel system of the zeolite because of the enhanced potential due to the proximity of the pore walls (i.e. micropore primary filling step due to adhesive forces). The uptake is very steep and the adsorption equilibration time is very long due to the hindered diffusion of N_2 molecules through constrictions (the 8-ring openings) of molecular size dimensions. This is followed by a more gradual filling of the porous structure (supermicropore filling) that gives rise to the knee of the isotherm (i.e. there arises the micropore secondary filling stage due to cohesive forces between ad-molecules) at relative pressures between 10^{-4} and 10^{-2}. Lamellar impurities contribute to the adsorption at higher pressures and are responsible of the narrow hysteresis loop that is observed along this region.

3.3. Clinoptilolites

Nitrogen sorption isotherms of clinoptilolites (CLIN and CLIM) are shown in Fig. 6. The adsorption isotherm of sample CLIM in logarithmic p/p^0 scale is shown in Fig. 12. Argon sorption at 76 K on sample CLIM is shown in Fig. 9 and the logarithmic p/p^0 graph is shown in Fig. 12. The enhanced uptake capacity of the sample CLIN with respect to the natural material CLIM can be clearly observed in Fig. 6.

3.3.1. Nitrogen Sorption on Natural Clinoptilolite. The isotherm of the natural sample is IUPAC Type IV.

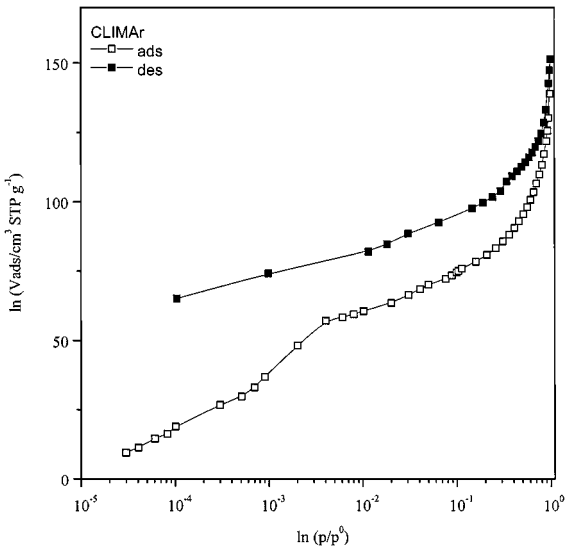

Figure 12. Ar sorption at 76 K on CLIM plotted in a logarithmic p/p^0 scale.

Along the channels of this zeolite there exist ions (i.e. Na^+, K^+, Ca^{++}) that do not allow the passage of N_2 molecules into them. The boundary ascending curve of the CLIN isotherm is about the same as a standard N_2 isotherm on a non-porous substratum. In fact the t-plot is linear along a large range of relative pressures (0.01–0.86) and the BET surface area is very close to the t surface area (13.6 vs. 15.47 $m^2\ g^{-1}$).

The natural substratum also allows for the presence of a small amount of impurities, especially clays, quartz and amorphous glassy material. This is confirmed by the H3 shape of the hysteresis loop with an inception point at around $p/p^0 = 0.4$. The impediment for N_2 to penetrate into the ultramicropores causes that low-pressure hysteresis be absent in this material.

3.3.2. Nitrogen Sorption on Modified Clinoptilolite. The extent of microporosity in the modified sample, CLIM is remarkable with respect to that of its ancestor natural sample. Acid treatment of this high-silica natural clinoptilolite has produced an improved or modified adsorbent, via the mechanisms of decationation and dealumination, and also by dissolving any amorphous silica blocking the channels in the structure. The cation blocking effect in this clinoptilolite is thus eliminated or lowered by acid treatment, i.e. substituting large ions by protons. Eventually a continued acid treatment also lowers further cation exchange by leaching Al_3^+ from framework positions while introducing H^+ into the few remaining cation locations. Dealumination by acid treatment can be seen in Table 2 where the Si/Al weight ratio is larger for CLIM than for its ancestor CLIN (5.71 vs. 5.22).

The CLIM isotherm presents a very wide and open hysteresis loop that extends over the whole pressure range (Fig. 13). The hysteresis cycle includes both high and low-pressure hystereses. The low-pressure hysteresis may be linked to the irreversible retention of N_2 molecules around micropore necks or corners that exist around the intersections between channels A, B and C. The microporous volumes of clinoptilolite CLIM obtained from t- and DR plots respectively are shown in Table 4. While the natural sample has a non-accessible microporous structure to the adsorptive nitrogen molecules, the modified substratum presents an important micropore contribution to the total adsorption. The microporous volumes calculated by the t-plot and the DR plots are in good agreement (0.1236 vs. 0.1575 $cm^3\ g^{-1}$).

The A_{ext} calculated from the t-plot is much higher in the modified specimen than in the natural one. This

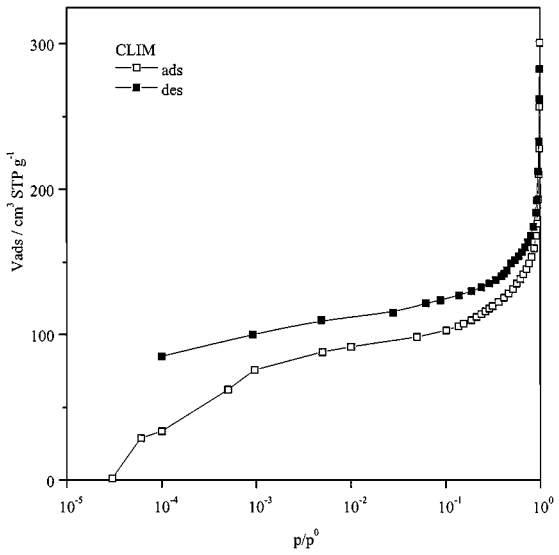

Figure 13. N_2 sorption at 76 K on CLIM plotted in a logarithmic p/p^0 scale.

points out that concomitantly with the opening of the micropore structure there arises an enhancement of the mesoporosity. The external surface areas calculated by the *t* or BET plots are close to each other for both natural and modified specimens. The external BET area displays a remarkable linearity in the range $p/p^0 = 0.05$–0.31 as found by Remy and Poncelet (1995).

3.3.3. Argon Sorption on Modified Clinoptilolite. Aiming to evidence the possibility that low-pressure hysteresis may be due to any specific interaction between the nitrogen molecules and specific sites within the zeolitic substratum, argon adsorption was measured at 76 K on CLIM (Fig. 9). Results show that the hysteresis loop persisted wide and open through the whole pressure range (Fig. 12) as in the case of N_2. The logarithmic plot of the isotherm shows a notable uptake enlargement at around p/p^0 5×10^{-4}–5×10^{-3}. The linearity of the DR plot is attained between a wide range of relative pressures, i.e. 3×10^{-5} to 4×10^{-3}. In this plot the adsorption energy at low pressures (initial slope) is sensibly smaller when compared with nitrogen, suggesting that a weaker interaction between the substratum and the argon molecules. Nevertheless the low-pressure hysteresis remains and so the existence of a gate effect (stronger adsorption at micropore necks) is very likely to persist causing the occurrence of long equilibration times.

The BET area of the sample measured by argon is rather different than that calculated from nitrogen, however the isotherms look very similar except at high pressures. Subtraction of the micropore volume to the adsorption data renders very good BET plots, the linearity improves and the pressure range extends whilst agreement with the *t* area becomes very good.

3.3.4. The Filling Mechanism of the Microporous Structure of CLIM. It is important to note that the N_2 isotherm of CLIM is not smooth (Fig. 13) especially at low pressures. A high-resolution *t*-plot (see Fig. 14) visualizes a series of filling stages during the uptake of adsorptive molecules. Adsorption may be really strong around the channel intersections, where edges and micropore necks arise, the initial slope of a DR plot is very large indeed at low relative pressures (i.e. $p/p^0 < 5 \times 10^{-5}$) denoting a high adsorption energy. There upon a more gradual adsorption takes place at low relative pressures between 5×10^{-5}–10^{-3}; pressure at which more moderate adsorption energies arise (this being evidenced by a smaller slope of the DR plot). In this region, the volume filling of channels A, B and C proceed concurrently and sequentially according to the dimensions of each channel. Complete volume filling of channel C will occur first causing a tenuous discontinuity, filling of channel B is next and ending with the total occupancy of channel A at higher pressures. Afterwards, filling of supermicropores essentially by cohesive forces takes place at around $p/p^0 \approx 10^{-3}$ to 10^{-2}. Filling of mesopores takes place from intermediate to very high relative pressures; at around $p/p^0 = 0.95$ the uptake becomes faster. It is important

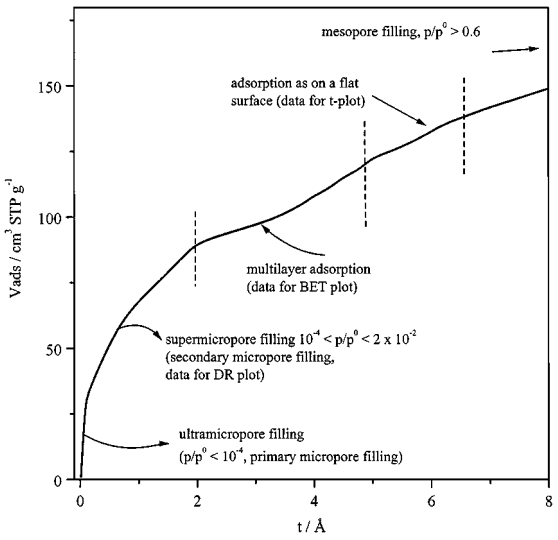

Figure 14. High-resolution *t*-plot for N_2 sorption at 76 K on CLIM.

to say that linearity of the DR plots occurs in the range of relative pressures between 5×10^{-5} and 10^{-3}, where a good agreement with the *t*-plot value is obtained (see Table 4).

3.4. Mordenites

3.4.1. Nitrogen Sorption on Natural Mordenite. N_2 adsorption-desorption isotherms at 76 K on (a) natural and (b) synthetic mordenite specimens are shown in Fig. 7. The isotherm of sample MORN is a combination of Types I and IV; the hysteresis loop is open and includes both narrow low- and high-pressure hysteresis loops. The shape H3 of the hysteresis cycle at high pressure suggests that a small amount of non-crystalline materials of lamellar type (i.e. natural clays) exist in between the crystallites.

The adsorption isotherm of the natural mordenite MORN is sloping between $p/p^0 = 3 \times 10^{-5}$ and 0.90 where adsorption is sensibly smaller than that developed on the synthetic sample MORS. Steep adsorption occurs at very low relative pressures ($<3 \times 10^{-5}$) and a very good DR plot is obtained at p/p^0 between 4×10^{-5} and 10^{-2}. DR slopes at lower pressures ($<3 \times 10^{-5}$) indicate stronger adsorption energies. The BET plot is linear between $p/p^0 = 0.05$ to 0.20 while the *t*-plot is so between $p/p^0 = 0.02$ to 0.40.

3.4.2. Argon Sorption on Natural Mordenite. Argon sorption on natural mordenite is similar to nitrogen sorption. The isotherm (Fig. 10) displays an open and slightly wider hysteresis loop compared to the case of nitrogen. However adsorption is not as sharp at low relatives pressures as it is with nitrogen, it happens that cation interactions with Ar are weaker than with N_2. Again there is evidence of the existence of lamellar impurities in the sample.

The DR plot is linear between $p/p^0 = 5 \times 10^{-4}$ and 0.02 while the BET plot is linear between $p/p^0 = 0.05$ and 0.26. The BET and *t*-surface areas are lower for Ar than for N_2. This is presumably due to the uncertainty about the area occupied by Ar on different substrata and that has been found to vary between 13.8 and 18 Å^2 (Gregg and Sing, 1982).

3.4.3. Nitrogen Sorption on Synthetic Mordenite. The isotherm of this sample corresponds to a Type I and shows a very steep sorption uptake at very low pressures. This saturation region (in the sense that all micropores are already filled) extends between $0.1 < p/p^0 < 0.9$. At higher relative pressures there is still no substantial increase of the sorption capacity, thus indicating that the sample is very pure indeed since no mesopores are present as neither multilayer adsorption nor capillary condensation develops therein. However, low-pressure hysteresis can also be observed in the synthetic sample as with the natural samples. Formally the microporous network of mordenite is two dimensional, however the structure is practically considered as an array of one-dimensional parallel channels (Chiang et al., 1997) with apertures made of 12-membered rings. Molecular diffusion along channel 2 involves capillaries having 8-membered ring elliptical apertures with very small free diameters that are often occupied by cations and that are impossible to be trespassed by nitrogen. The low-pressure hysteresis phenomenon is very likely to be due to an irreversible retention of N_2 molecules around necks or pore corners throughout the mordenite structure, remember that channels 2 are located as side pockets along the larger channels 1. The intersections between channels 1 and 2 are regions around strong irreversible adsorption may occur.

4. Conclusions

Natural zeolites, in contrast to synthetic materials, have a limited crystallinity thus indicating a certain degree of contamination of the structure with other minerals or amorphous glassy material. The presence of cations or minerals blocking the pore channels of a zeolite and the limited extent of its crystalline structure, drastically reduce its sorption activity by diminishing the microporous volume accessible to the adsorbate. Acid treatment of a high-silica natural clinoptilolite produces an improved adsorbent. A distinctive characteristic of modified clinoptilolite and mordenite samples, is the irreversible adsorption of nitrogen at pore entrances that gives origin to low-pressure hysteresis; in erionite samples no such phenomenon arises.

Nomenclature

a, b, c	Crystallographic axes
a_m	Area occupied per molecule
A_B	BET surface area
A_{Bext}	BET external surface area
A_{ext}	External surface area
A_t	*t*-plot surface area
C_B	BET constant

C_{Bext}	BET constant for adsorption on the external surface
CLIN	Natural clinoptilolite
CLIM	Modified clinoptilolite
DR	Dubinin-Radushkevich
E_0	Characteristic adsorption energy of the adsorbent
ERIN	Natural erionite
ERIS	Synthetic erionite
MORN	Natural mordenite
MORS	Synthetic mordenite
p	Pressure
p^0	Saturation vapour pressure
R	Gas constant
T	Temperature
t	Thickness of the adsorbed layer
W	Microporous volume filled at pressure p
W_{0t}	Micropore volume obtained from a t-plot
$W_{0\text{DR}}$	Micropore volume obtained from a DR plot
$W_{0\text{DRC}}$	Micropore volume obtained from a DR plot considering adsorption on the external surface

Greek Symbols

α, β, γ	Unit cell parameters
α_s	Sing's α_s method of analysis

Acknowledgments

Thanks are due to the National Science and Technology Council of Mexico (CONACyT) for financial support through the projects 960502003 and 28416-E.

Note

1. We are indebted to Dr. Bergk from the Universidad Autónoma de Puebla for kindly providing this sample.

References

Breck, D.W., *Zeolite Molecular Sieves*, p. 60, Wiley, New York, 1974.

Chiang, A.S.T., C.K. Lee, W. Rudzinski, J. Narkiewicz-Michalek, and P. Szabelski, "Energy and Structure Heterogeneities for the Adsorption in Zeolites," *Equilibria and Dynamics of Gas Adsorption on Heterogeneous Solid Surfaces*, W. Rudzinski, W.A. Steele, and G. Zgrablich (Eds.), pp. 519–572, Elsevier, Amsterdam, 1997.

Dubinin, M.M. and V.A. Astakhov, "Description of Adsorption Equilibrium of Vapors in Zeolites over a Wide Range of Temperature and Pressure," *Adv. Chem. Ser*., 102, p. 69, Am. Chem. Soc., Washington, D.C., 1971.

Gregg, S.J. and K.S.W. Sing, *Adsorption, Surface Area and Porosity*, Academic Press, London, 1982.

Inagaki, M. and M. Sunahara, "Pore Formation in Carbons Derived from Phenol Resin and their Gas Adsorption," *Characterization of Porous Solids IV*, B. McEnaney, T.J. Mays, J. Rouquerol, F. Rodríguez-Reinoso, K.S.W. Sing, and K.K. Unger (Eds.), pp. 156–162, The Royal Society of Chemistry, Cambridge, 1997.

Jacobs, P.A. and J.A. Martens, *Synthesis of High-silica Aluminosilicate Zeolites*, pp. 321–323, Elsevier, Amsterdam, 1987.

Kaneko, K., "Heterogeneous Surface Structures of Adsorbents," *Equilibria and Dynamics of Gas Adsorption on Heterogeneous Solid Surfaces*, W. Rudzinski, W.A. Steele, and G. Zgrablich (Eds.), pp. 679–714, Elsevier, Amsterdam, 1997.

Maddox, M.W., N. Quirke, and K.E. Gubbins, "Simulation of Pore Blocking Phenomena in Model Porous Networks," *Characterization of Porous Solids IV*, B. McEnaney, T.J. Mays, J. Rouquerol, F. Rodríguez-Reinoso, K.S.W. Sing, and K.K. Unger (Eds.), pp. 65–72, The Royal Society of Chemistry, Cambridge, 1997.

Mather, R.R., "Analysis of Pore Properties from Low Pressure Hysteresis in Nitrogen Adsorption Isotherms," *Characterization of Porous Solids IV*, B. McEnaney, T.J. Mays, J. Rouquerol, F. Rodríguez-Reinoso, K.S.W. Sing, and K.K. Unger (Eds.), pp. 314–318, The Royal Society of Chemistry, Cambridge, 1997.

Michiels, P. and O.C.E. De Herdt, *Molecular Sieve Catalysts*, EPO Applied Technology Series, Vol. 9, Pergamon Press, Oxford, 1987.

Remy, M.J. and G. Poncelet, "A New Approach to the Determination of the External Surface and Micropore Volume of Zeolites from the Nitrogen Adsorption Isotherm at 77 K," *J. Phys. Chem*., **99**, 773 (1995).

Sing, K.S.W., D.H. Everett, R.A.W. Haul, L. Moscou, R.A. Pierotti, J. Rouquerol, and T. Siemieniewska, "Reporting Physisorption Data for Gas/Solid Systems," *Pure Appl. Chem*., **57**, 603–619 (1985).

Stoeckli, F., A. Lavanchy, and D. Hugi-Cleary, "Dubinin's Theory: A Versatile Tool in Adsorption Science," *Fundamentals of Adsorption 6*, F.A. Meunier (Ed.), pp. 75–80, Elsevier, Paris, 1998.

Tsitsihvili, G.V., T.G. Andronikashvili, G.N. Kirov, and L.D. Filizova, *Natural Zeolites*, Horwood Ellis, New York, 1992.

WADD Technical Report 60-56, A Compendium of the Properties of Materials at Low Temperature (Phase I), V.J. Johnson (Ed.), Wright Air Development Division, United States Air Force, Wright-Patterson Air Force Base, Ohio, 1961.